NUMERICAL INVESTIGATION OF FLOW IN UAV SINUSOIDAL COMPRESSOR STAGE

Bartosz BOGUCKI, MSc
Institute of Aviation, Warsaw, Poland
Engineering Design Center

Summary

Centrifugal compressors, which have lost their application in the military crew airplanes, are often implemented to small-dimension unmanned aircraft engines. Their one-stage high-pressure ratio, low-complexity construction and relatively small dimensions and weight consolidated their position in modern constructions. Continuous development of these compressors has attracted increased attention to the flow field in smaller and fast-rotating blade passages. Supersonic phenomena, mixing losses and unsteadiness of the flow in the impeller are expected to be studied with more details.

The work presented in this report was performed at the Ecole Nationale Supérieure d'Ingénieurs of Constructions Aéronautiques (ENSICA) in Toulouse within an UAV engine development program led by Department of Fluid Mechanics, ENSICA and JPX Company, France.

The purpose of this study was to investigate numerically several design solutions implemented to mixed-flow compressor stage of the 100kN turbojet engine named T100.

1. INTRODUCTION

At the beginning of conception work on the T100 engine, an 18-blades sinusoidal (mixed-flow) compressor with 9 splitters was designed (Figure 1). The main objective in placing additional blades in flow passage of the machine was to adapt as much as possible the geometry to supersonic flow expected at the inlet. Hence, from 18 full–length blades, half of them were cut at some distance from the blade leading edges to enlarge inlet throat, and as result avoid choke problems in this region. However, during experiments it occurred that the inlet conditions are subsonic and that the front section of the impeller does not have to be designed so restrict. Thus, as a method to reach higher stage efficiency it was proposed to replace the splitters by full–length blades. In the impeller without splitter more uniform flow in the blade passage, and consequently higher efficiency were expected. As the result of the two concepts, a necessity of their comparison took place.

Next improvement introduced to the compressor's design was reducing tip clearance to minimum. It was possible due to new material applied on the shroud surface, which allowed to match the blade tips up with the shroud surface by wearing down used material from the internal shroud surface (abradable process). Therefore, need of numerical trade-off study of the tip clearances effect on performance occurred.

The last analysis was dedicated to choke effect occurring in the non–splittered compressor.

Since this phenomenon has crucial significance for the impeller performance and operating range, critical back static pressure and respective mass flow rate within compressor had to be known.

The NUMECA software was used for this project. The package is highly sophisticated tool dedicated for design, analysis and optimization of turbomachinery. NUMECA provides many useful features regarded to mesh generation (IGG/AutoGrid), solving (FINE/Turbo) and post-processing (CFView) of turbomachine CFD models.

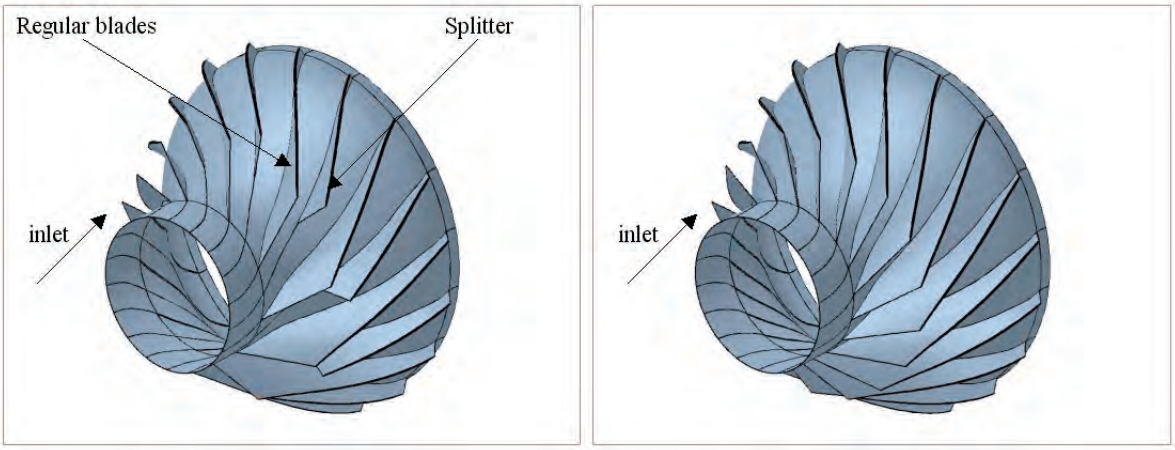

Fig. 1. Mixed-flow compressor stage with splitter (left) and without splitter (right)

2. THEORETICAL ASPECTS

To enable comparison of the two analyzed compressor designs, it is worth to define few important operating parameters that characterize turbomachines.

2.1 Efficiency

For all turbomachines efficiency is defined as ratio of work inputs into ideal and actual compressors, which have equal pressure rise [2]:

$$\eta = \frac{L_{isentr}}{L_{actual}} \tag{1}$$

In adiabatic processes work input is equal to the rise in stagnation enthalpy:

$$L = h_{02} - h_{01} \tag{2}$$

Then, the efficiency is defined as:

$$\eta_{isentr} = \frac{h_{02isentr} - h_{01}}{h_{02} - h_{01}} \tag{3}$$

After introducing uncomplicated thermodynamics expressions for the enthalpy we receive simple expression for the isentropic efficiency [2]:

$$\eta_{isentr} = \frac{\left(p_{02}/p_{01}\right)^{(\gamma-1)/\gamma} - 1}{\left(T_{02}/T_{01} - 1\right)} \tag{4}$$

However, definition of the isentropic efficiency has one major disadvantage, i.e. it gets lower as the overall pressure ratio increases. It can be avoided by using another expression for efficiency in adiabatic compressors, called polytrophic efficiency. It removes the mentioned penalty so that compressors of the same aerodynamic quality, but significantly different pressure ratio, would have the same polytropic efficiency [2]:

$$\eta_{politr} = \frac{\gamma - 1}{\gamma} \frac{\ln\left(p_{02}/p_{02}\right)}{\ln\left(T_{02}/T_{01}\right)} \tag{5}$$

2.2 Slip effect

Since the compressor stage consists of rotating components we can distinguish two frames of reference: the absolute frame where velocity is related with stationary coordinate system and the relative frame is moving at the local blade speed. In these two frames we can consider relative and absolute velocities which throughout this report are denoted by *W* and *C*, respectively. The velocity triangles can be built using the vector relation: relative velocity + blade speed = absolute velocity [1]. Velocity triangles at the inlet and the outlet of the impeller are shown in Figure 2. Relative flow angle is denoted by β and absolute flow angle by α and they express inclination of the relevant velocity vectors from axial direction. Moreover, each velocity vector is usually decomposed onto components parallel to principal axes of compressor: meridional and tangential.

The designers of centrifugal impellers are interested in the real flow direction relative to the blades because in the impeller–exit area the flow direction does not follow blade geometry and deviates significantly. In general, the mean flow angle β_2 is lower then the blade angle β_{2b}. The difference between the two is called a slip angle, β_2, and the effect itself is usually called a slip effect in impeller. Due to the slip effect the pressure ratio is often lower than theoretically predicted [3].

2.3 Non-dimensional parameters

Non–dimensional design parameters allow describing the overall performance of the machine so that assessment and comparison between compressors with different dimensions and flow parameters can be easily made. The first and the most obvious dimensionless parameter is static or total pressure ratio which expresses ability of the compressor to rise the pressure in the impeller [8]:

$$\bar{\pi} = \frac{p_{02}}{p_{01}} \tag{6}$$

The nominator in the given formula is the stagnation pressure at outlet of the impeller and denominator is the stagnation pressure at inlet. The choice of either static or stagnation pressure depends on the designer. Second non–dimensional parameter, which for isentropic process can be derived directly from pressure ratio, is temperature ratio [8]:

$$\bar{\tau} = \frac{T_{02}}{T_{01}} \tag{7}$$

Non-dimensional mass flow is the next crucial parameter deciding about compressor performance. It is expressed as [2]:

$$\Theta = \frac{\dot{m}\sqrt{T_{01}}}{p_{01}} \tag{8}$$

Then, mass flow corrected to standard conditions expresses as [2]:

$$\Theta_{corr} = \Theta \sqrt{\frac{T_{01}}{T_{ref}}} \frac{p_{01}}{p_{ref}} \tag{9}$$

where p_{ref}=101300 Pa and T_{ref}=288K is a reference standard atmospheric pressure at zero sea level.

2.4 Choke Flow in Compressor

Choke flow, also recalled as 'critical flow', is a special effect in compressor when due to sonic conditions in passage higher flow velocity cannot be reached. In gas flow through orifice there is a specific downstream/upstream pressure ratio for which the gas velocity reaches sonic conditions. At this point no information can be transmitted upstream through the nozzle and any further increase of the backpressure produces no increase of the mass flow and the flow becomes choked. However, mass flow can still increase due to rise of upstream pressure. As the inlet air pressure builds up, the density of the fluid also increases and since the mass flow is also a function of density, the mass flow rate increases linearly with inlet pressure [7].

The best experimental approach to create a 'choke map' for compressor is decreasing back static pressure to critical value and measuring corresponding mass flow and pressure ratio. Obtained function of pressure ratio in terms of mass flow rate is the compressor path to choke. In numerical simulation sonic conditions are achieved similarly, by lowering backpressure from value of 110% of the nominal static pressure to a point where choke is reached.

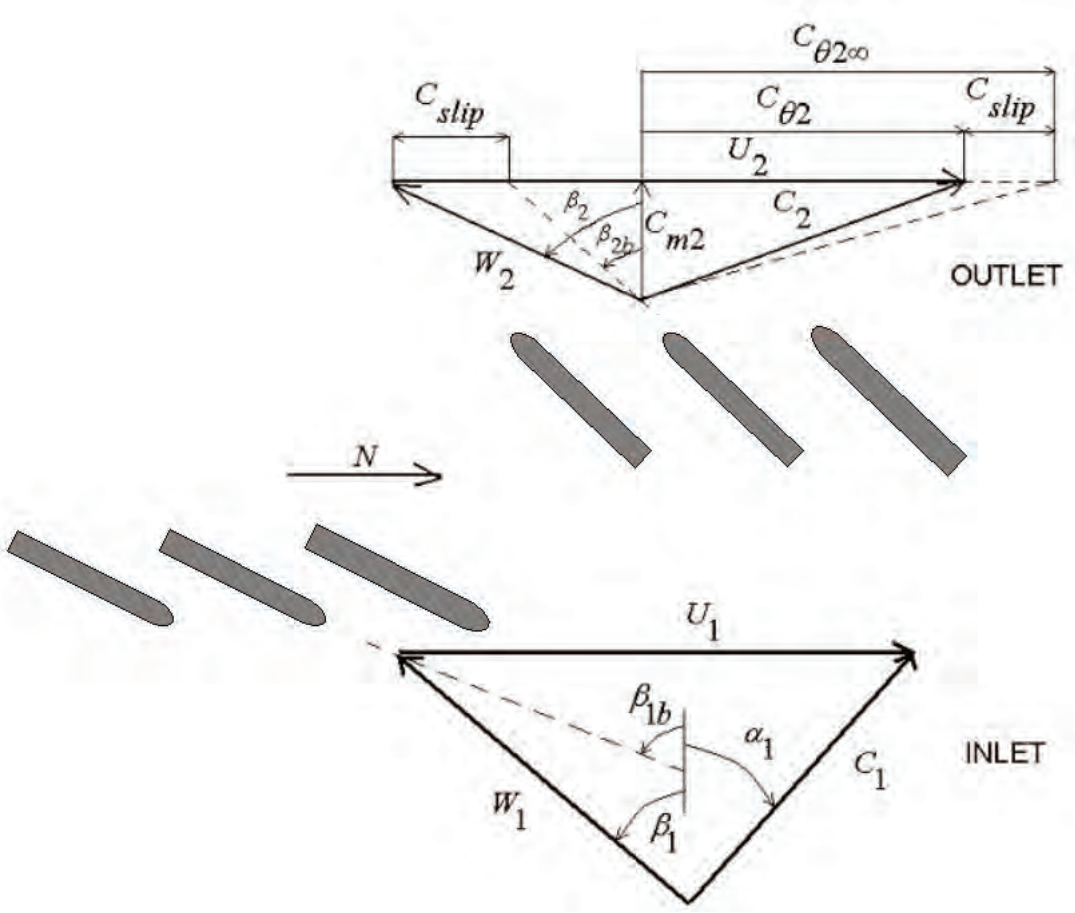

Figure 2. Velocity triangles at inlet and outlets of compressor stage

3. NUMERICAL MODELLING

Computational mesh was generated by means of the IGG/AutoGrid software. In the following turbomachinery studies the overall number of grid points ranges between 330,000 for the non-splittered compressor passage up to 950,000 for the splittered compressor passage (Figures 3 and 4). Special attention was paid to the high gradient regions like leading– and trailing–edges and to the first cell width along all solid boundaries of the profile (Figures 5 and 6).

To assess influence of turbulence model used in calculations, appropriate trade-off study for one test-case (non–splittered centrifugal compressor stage with no tip clearance) was performed. Pressure and temperature ratios and efficiencies computed during this examination are

compared in Table 1. It can be clearly seen, that the specified values for Baldwin–Lomax model differs from that for mutually similar Spalart–Allmaras and k-ε models. Having in mind that the one-equation Spalart–Allmaras turbulence model connects low numerical expenses with relatively good accuracy, this particular model was chose for all the computations. Values of y+ vary between 15 and 60, which is fully acceptable range for the Spalart-Allmaras turbulence model.

Table 1. Comparison of results for three different turbulence models

Turbulence Model	Pressure Ratio	Temperature Ratio	Isentropic Efficiency
Baldwin–Lomax	4.535	1.556	0.971
Spalart–Allmaras	4.464	1.572	0.931
Standard k-ε	4.483	1.566	0.945

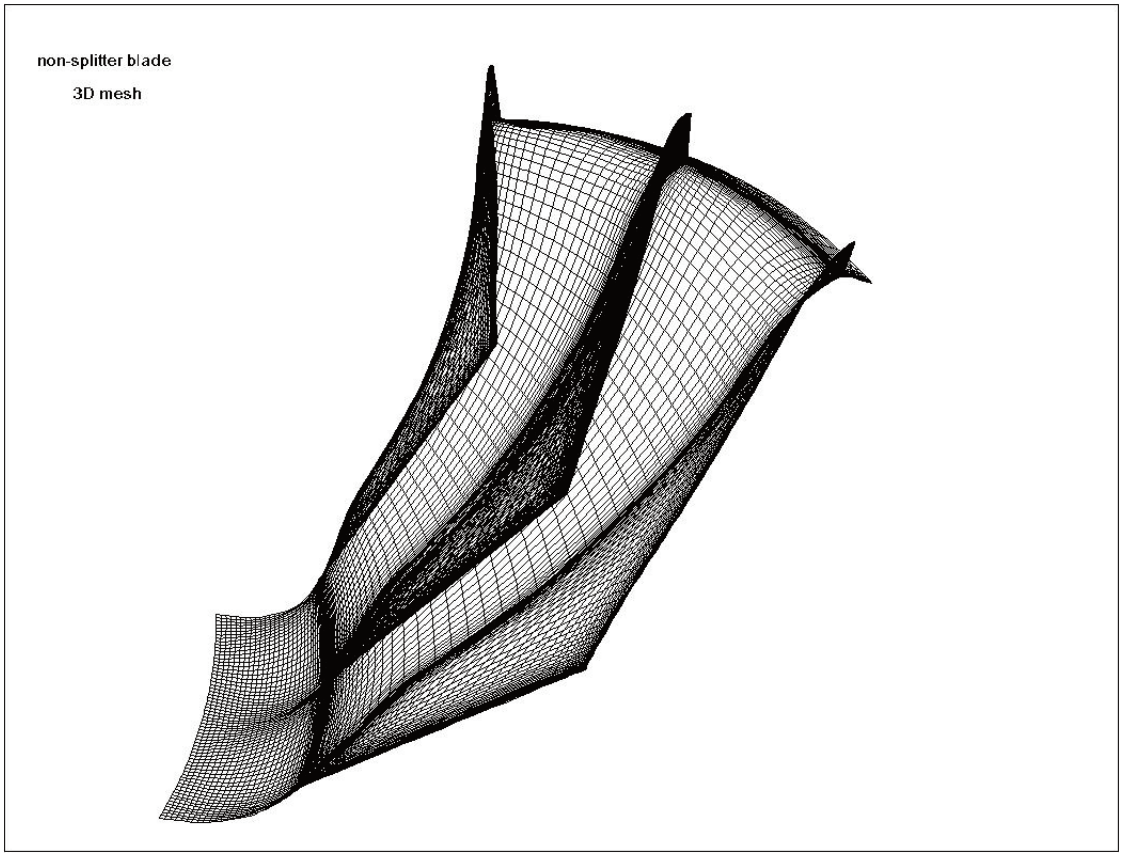

Figure 3. 3D mesh for non-splittered compressor passage

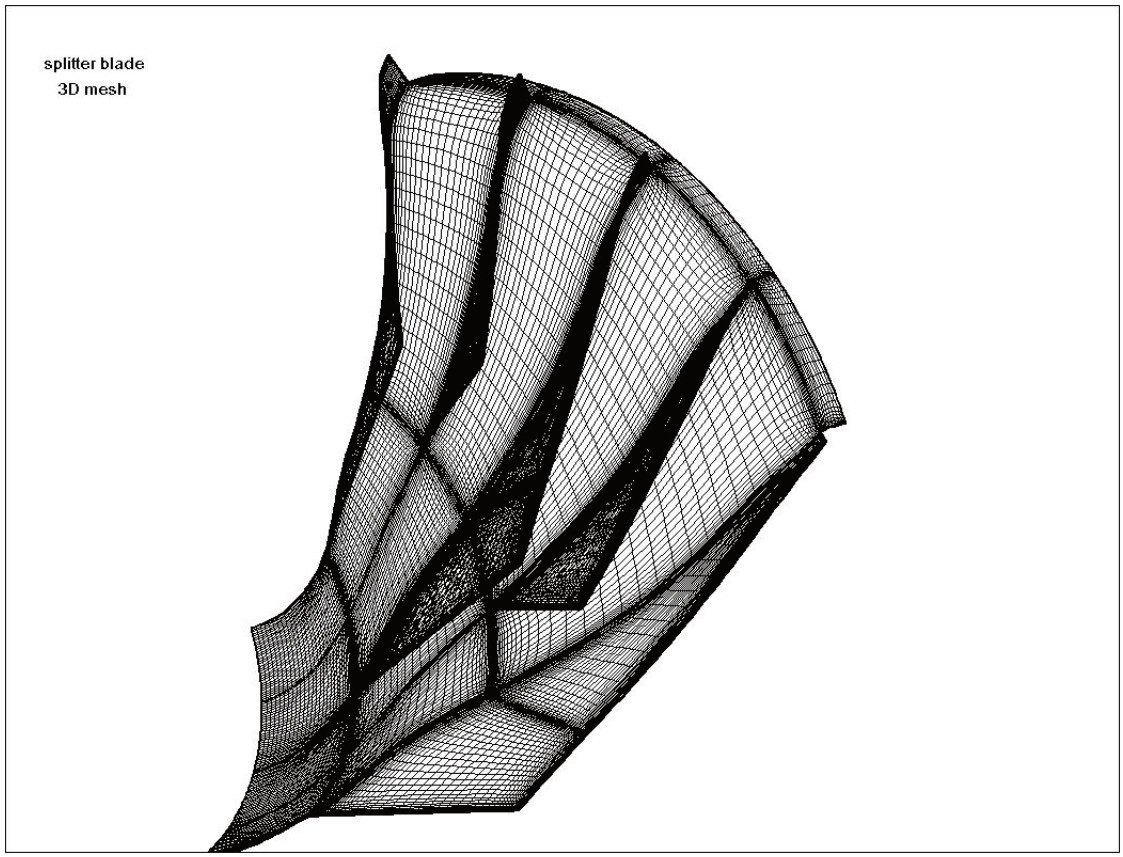

Figure 4. 3D mesh for splittered compressor passage

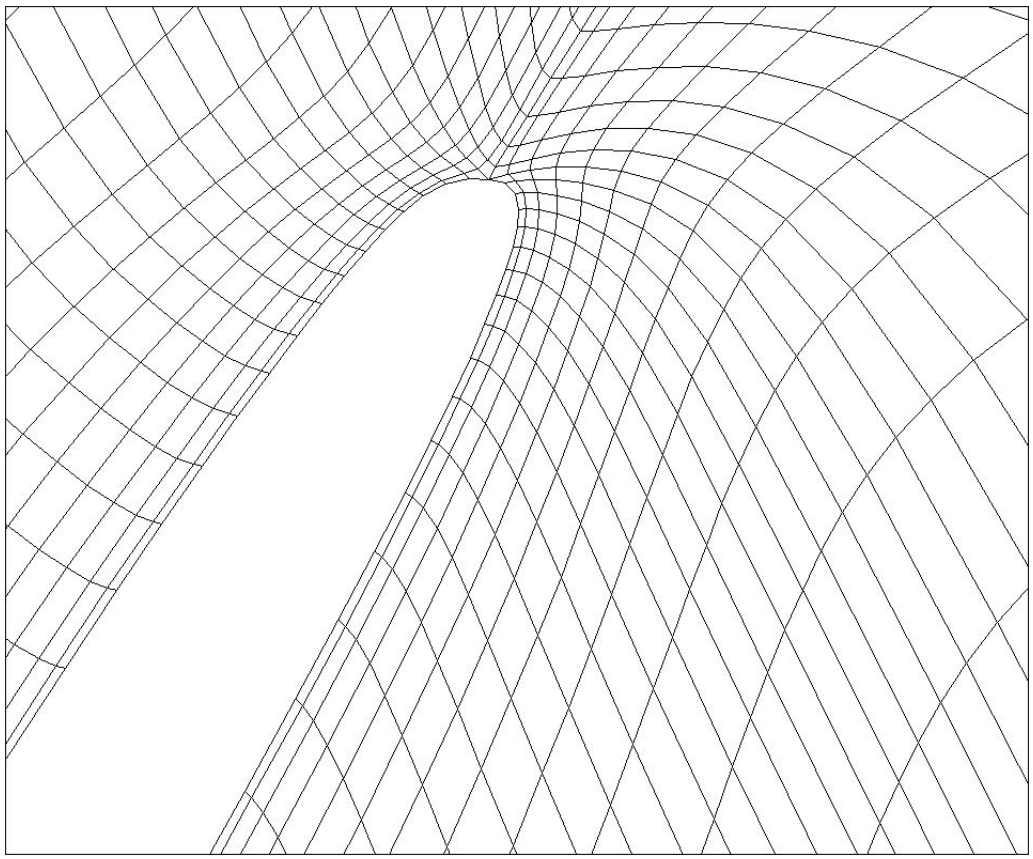

Figure 5. Clustering near the blade trailing edge

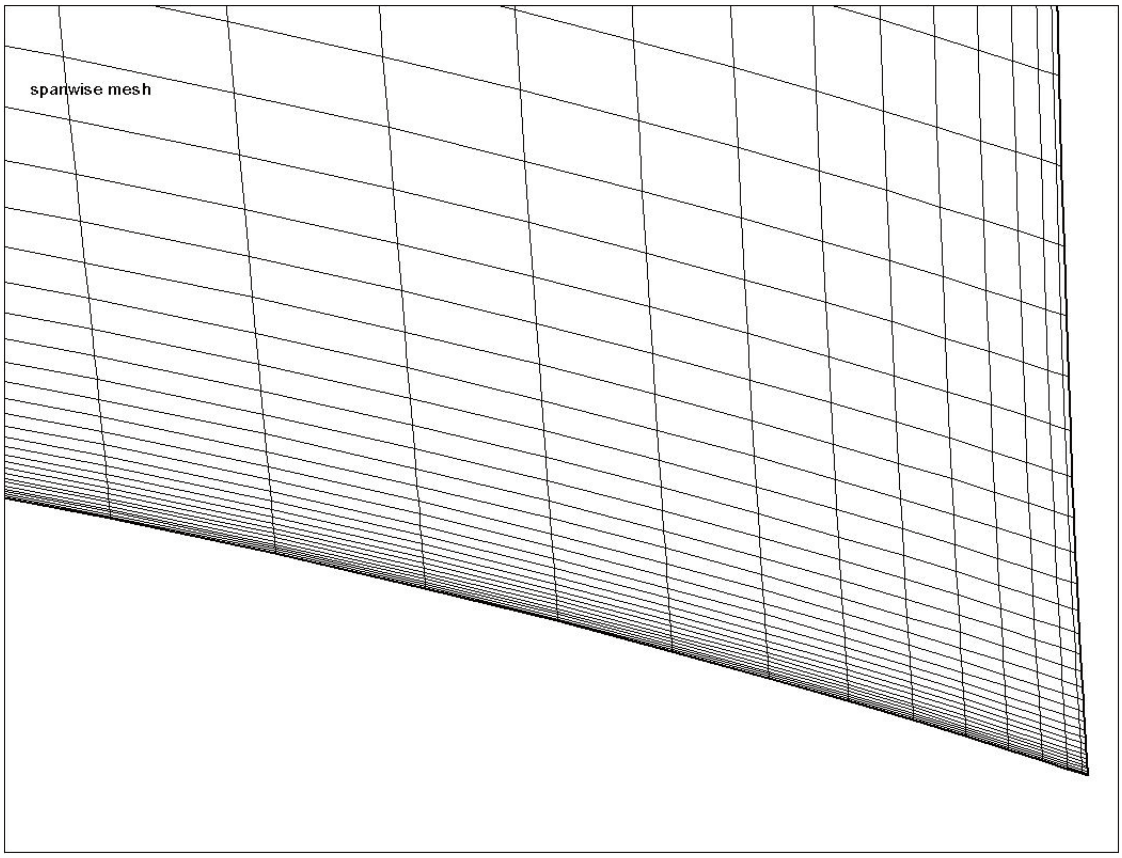

Figure 6. Near wall mesh resolution

In order to model actual conditions occurred during lab test of the compressor, a total atmospheric pressure, temperature and flow angle at the inlet were imposed. At the outlet a static pressure with radial equilibrium law was imposed. Summary of boundary conditions applied to the models is shown in Table 2.

Table 2. Boundary conditions for sinusoidal compressor stage study

Case study	Inlet	Outlet
Splittered compressor stage	$p_{01} = 101300Pa$ $T_{01} = 288K$	$p_2 = 180kPa$
Non–splittered compressor	$p_{01} = 101300Pa$ $T_{01} = 288K$	$p_2 = 180kPa$
Choke flow effect	$p_{01} = 101300Pa$ $T_{01} = 288K$	$p_2 = 125 \div 195kPa$
Tip clearance effect	$p_{01} = 101300Pa$ $T_{01} = 288K$	$p_2 = 180kPa$

5. COMPARISON STUDY RESULTS

In Table 3 the most important quantities describing flow state at the inlet and outlet are presented. The first noticeable difference in flow parameters between the cases is the mass flow

rate, which in the splittered compressor is lower by 0.2kg/s. The reason of the worse performance of the splittered compressor is a noticeable swirl generated at the splitter blade leading edge (Figure 7), which proceeds mainly to the right-hand side part of the compressor. Therefore, the right-hand side channel is less loaded and it transports only 42% of the overall mass flow. Figures 8 and 9 show clear difference in the flow pattern between these two sides of the compressor. On meridional planes, located in the middle of each channel, an absolute dimensionless velocity, C_m/U_2, for the splitter-blade configuration is plotted. Figure 10 shows flow field plotted at the cross section plane located downstream the splitter blade leading edge, and in case of non-splittered solution, in the corresponding distance from the inlet. The wake generated at the splitter blade is clearly seen as it occupies around 30% of the right-hand side flow duct of the splittered blade impeller.

Less uniform and stable flow for splittered version of the compressor leads to lower total pressure ratio achieved at the exit of the splittered impeller. Moreover, this situation is accompanied by worse isentropic efficiency, which dropped from 0.839 for the non-splittered impeller to 0.817 for the splittered compressor. Slight distinctions can be noticed in relative and absolute outlet Mach numbers which in the non–splittered compressor are bigger due to less perturbation and mixing losses. More surprising differences can be observed in the flow angles values. For impeller without splitter blade absolute and relative flow angles are 9 and 1.6 degrees greater, in respective order. It implies changes in rotor-diffuser interaction, and hence difference in the flow angles should be taken into account during designing of succeeding diffuser.

Table 3. Global flow parameters for splittered and non–splittered compressor stage

Flow parameter	Splittered impeller	Non-splittered impeller
p_{01} [kPa]	101300	101300
T_{01} [K]	288	288
p_2 [kPa]	185737	185675
p_{02} [kPa]	374679	382660
T_2 [K]	367.6	364.2
T_{02} [K]	448	446.8
M_2	1.046	1.064
β_2 [deg]	-32.2	-30.6
α_2 [deg]	45.4	54.7
$\Delta\beta_2$ [deg]	23.8	25.4
$\dot{m}$ [kg/s]	1.68	1.88
Θ_{corr}	$2.814e^{-4}$	$3.149e^{-4}$
$\pi = p_{02}/p_{01}$	3.7	3.78
$\tau = T_{02}/T_{01}$	1.555	1.551
η_{isentr}	0.817	0.839
η_{politr}	0.847	0.866

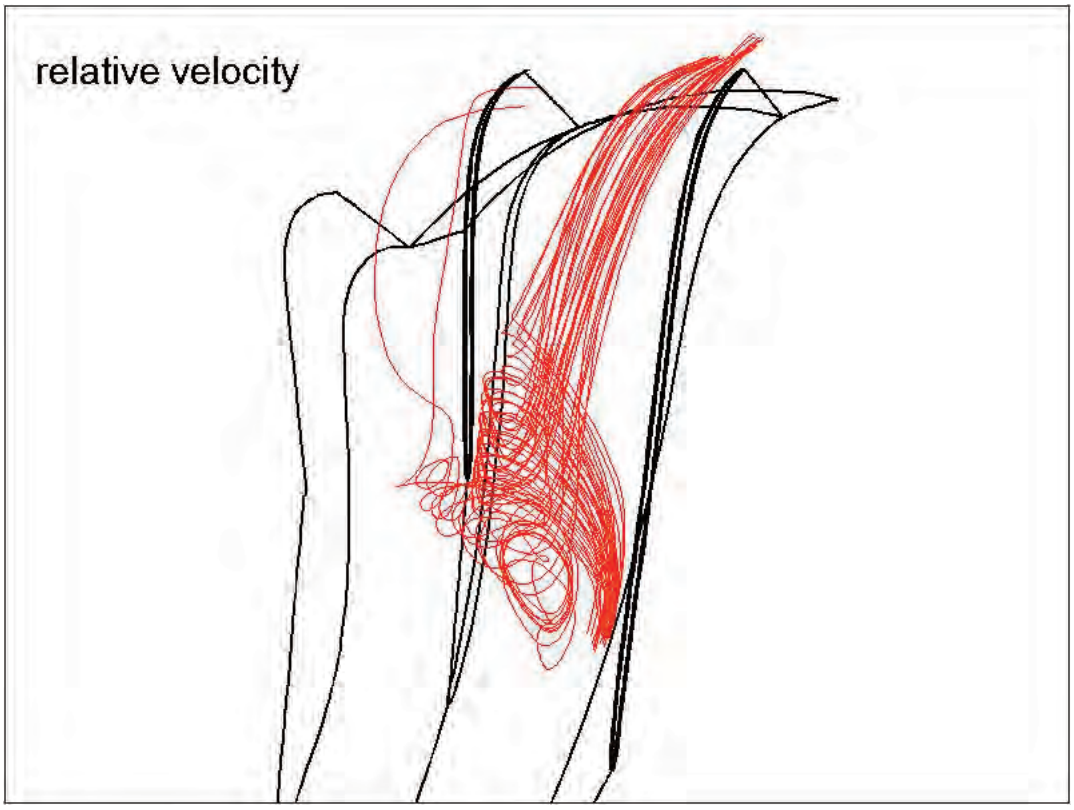

Figure 7. Swirl at the splittered compressor inlet

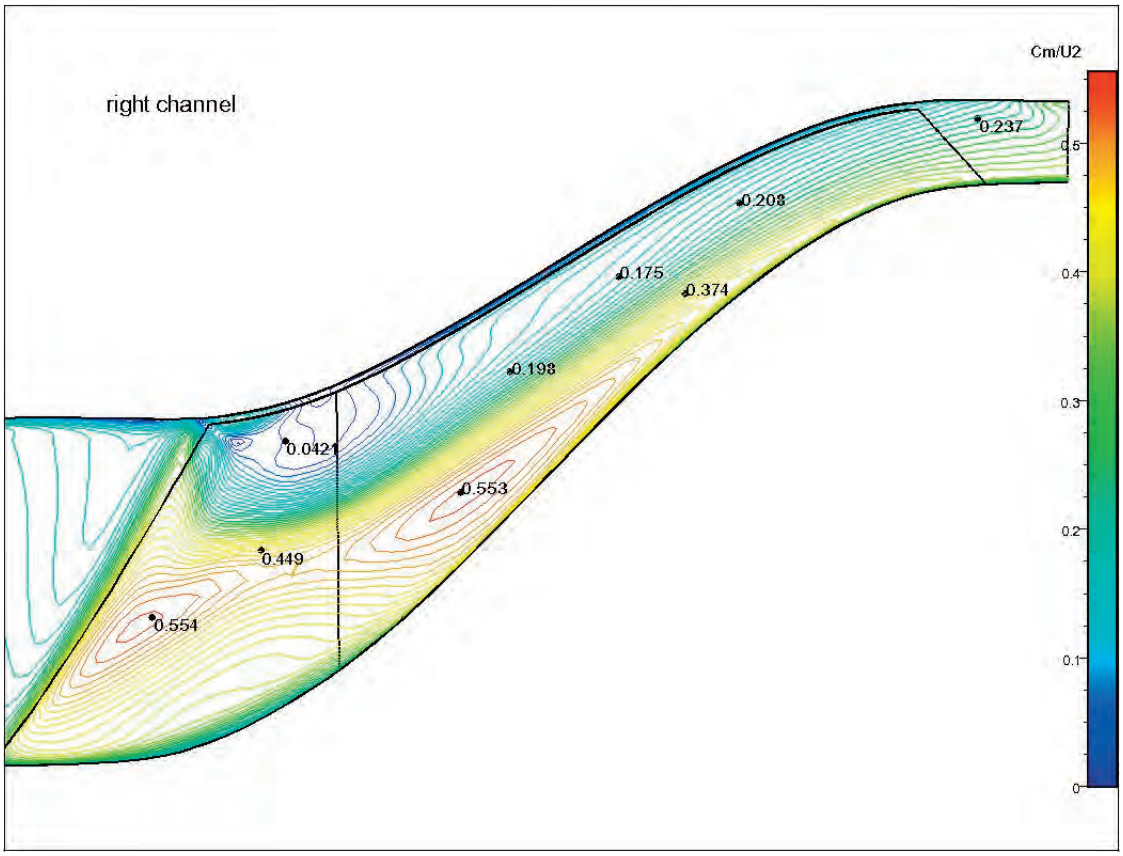

Figure 8. Flow pattern in the right-hand side channel of the splitter-blade impeller

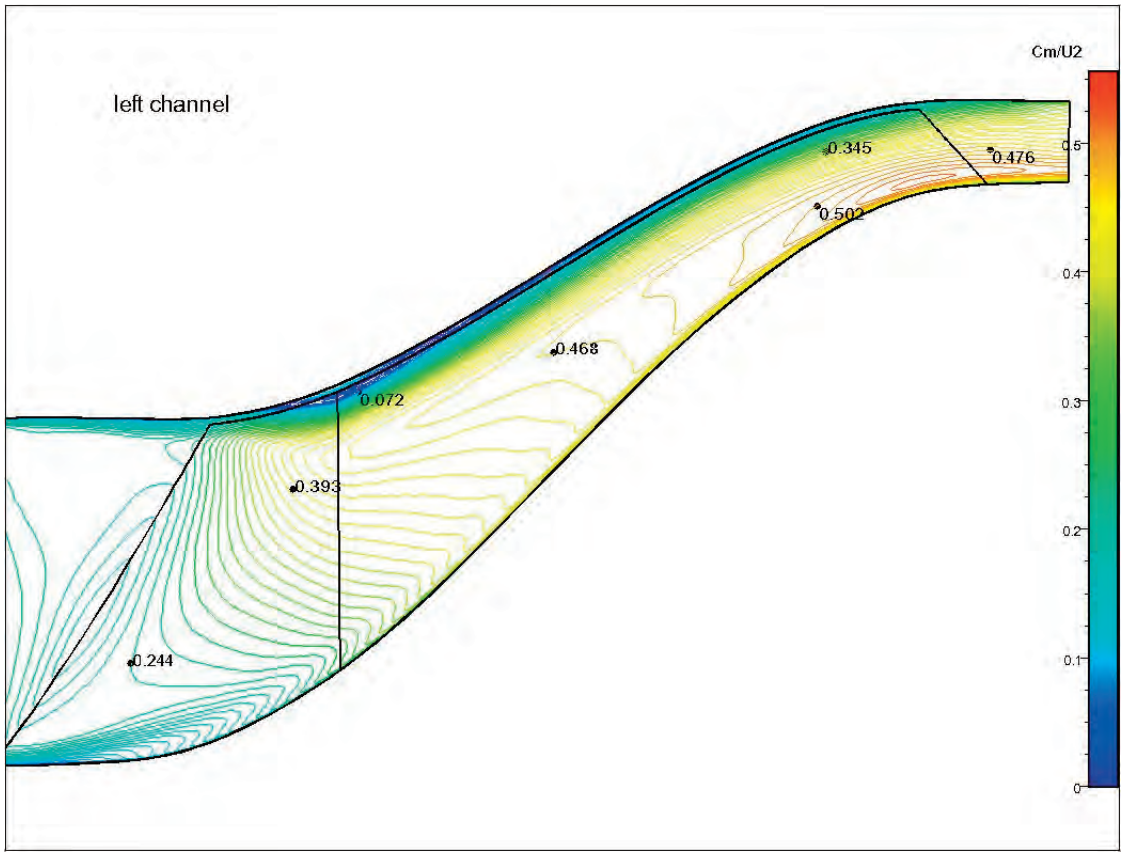

Figure 9. Flow pattern in the left-hand side channel of the splitter-blade impeller

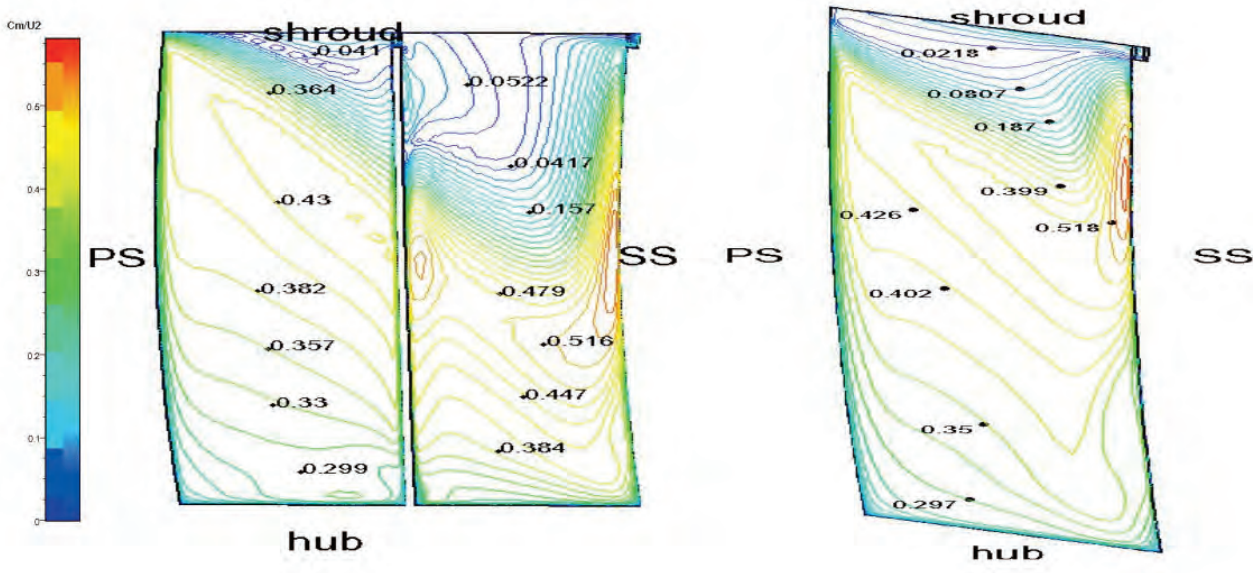

Figure 10. Flow pattern in cross-section of the impeller for splittered (left) and non-splittered (right) compressor stage. PS – pressure side; SS – suction side

6. TIP CLEARANCE EFFECT FOR NON-SPLITTERED COMPRESSOR

The numerical tests of the tip gap influence were done for the previously investigated non–splitter blade mixed-flow compressor stage with 18 blades and basic tip clearance of 0.6 mm.

The seven different values of the clearance gaps were examined. They were ranging between 0.0 and 1.0 millimetre (0.0, 0.1, 0.2, 0.4, 0.6, 0.8 and 1.0 mm). Regarding design conventions, the values were expressed in percents of blade height at outlet and were contained within 0 to over 15% of blade height.

Figure 11 reveals stagnation pressure contours at the impeller outlet for different clearances. The profile is plotted from shroud to hub. Significant decrement of the pressure magnitude from 450kPa to 390.2kPa with tip clearance rising is observed. Moreover, peak of the pressure value is shifting from the shroud towards to the centre of the channel. Slope of the pressure contour becomes steeper with higher negative gradient in hub direction. This clearly proves that flow path is affected not just near the shroud, as might be expected, but right across the passage.

Figure 12 illustrates pressure ratio change due to tip clearance rise. Again, evident linear drop in pressure ratio value from 4.1 to 3.67 can be noticed.

Figure 13 reveals values of isentropic efficiency. For tip clearance rising from 0.0 to 1.0 mm (0–15% of blade height) isentropic efficiency drops by over 7. The tendency of the function clearance–efficiency is almost linear, what agrees with literature. Moreover, the efficiency decrease rate confirms general rule, which states, that one point of stage efficiency is lost for an increment of passage clearance which is equal to 3% of the passage height at impeller discharge [4].

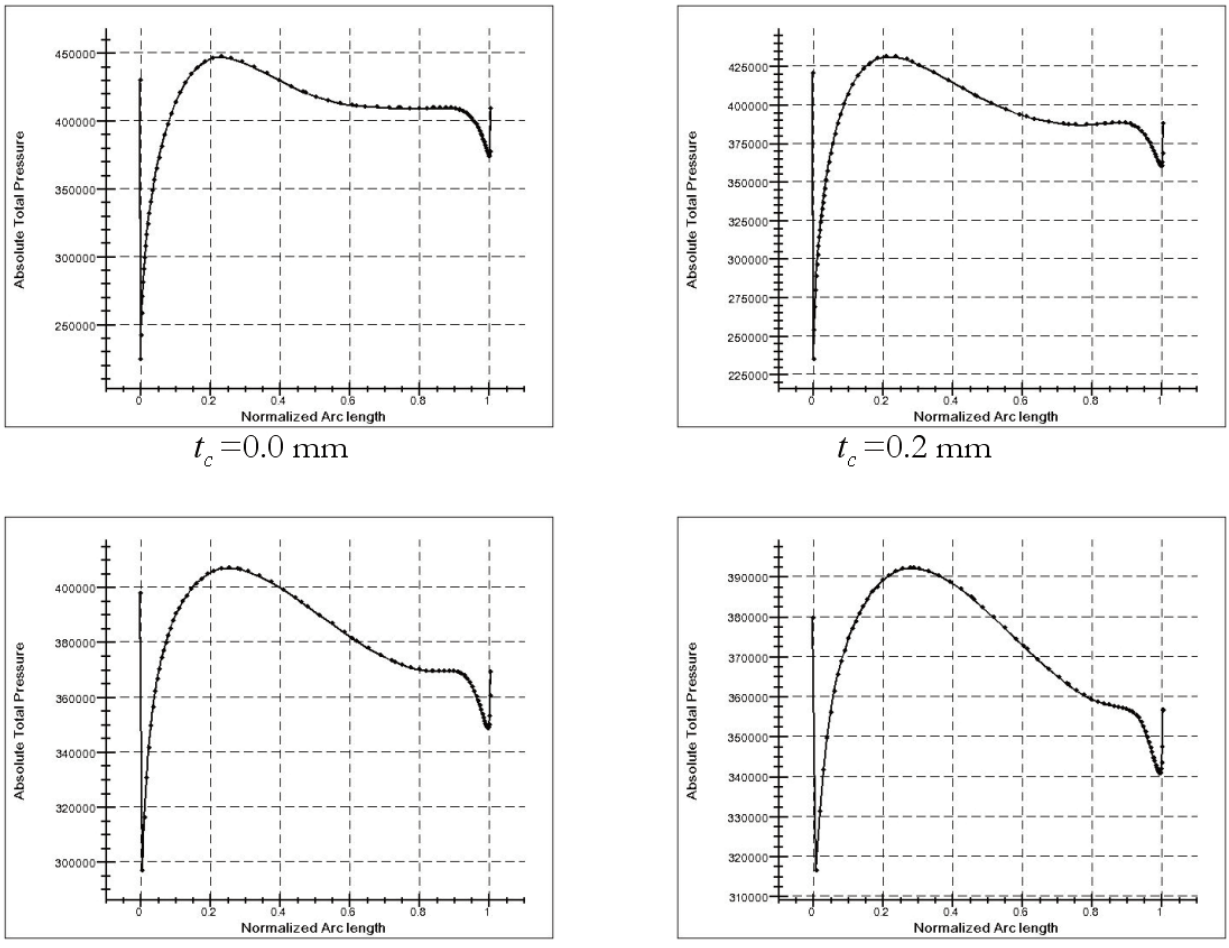

Figure 11. Total pressure profile at the impeller outlet for different tip clearances t_c

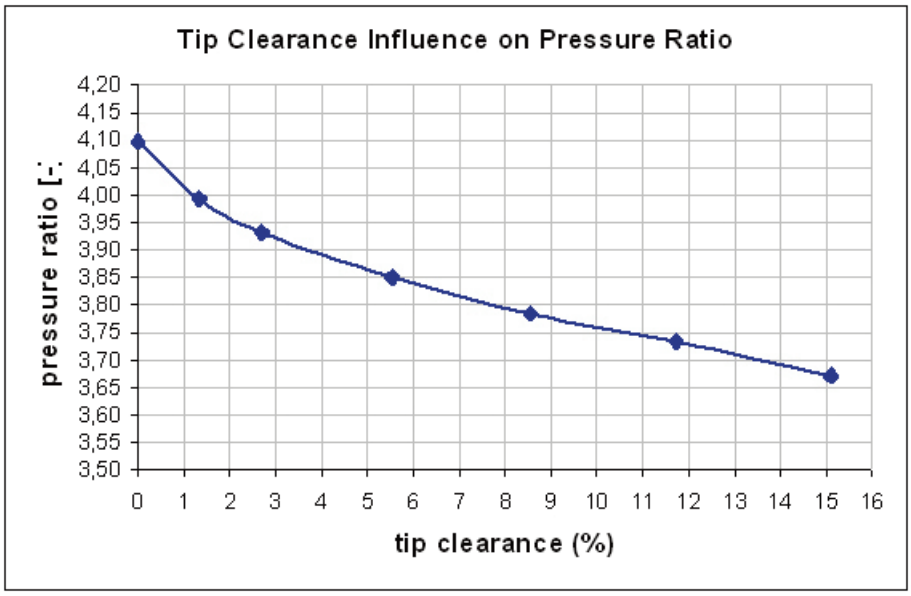

Figure 12. Pressure ratio for different tip clearance in non-splittered compressor

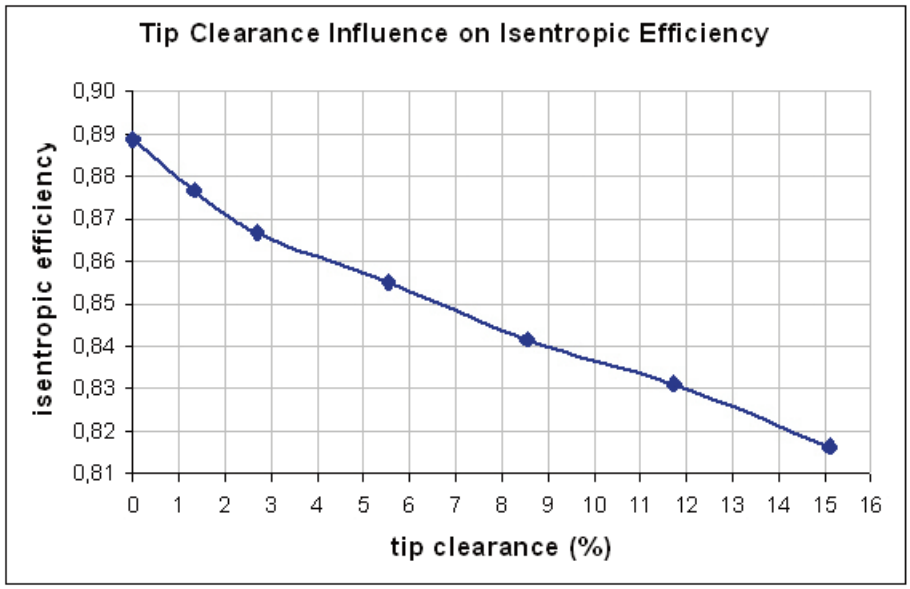

Figure 13. Influence of tip clearance on isentropic efficiency

7. COMPRESSOR MAP TO CHOKE

The model was the non–splitter centrifugal compressor stage with tip clearance 0.6mm and maximum pressure ratio of 3.85:1 and mass flow rate 1.88kg/s for 45000RPM.

In Figure 14 corrected mass flow rate and total pressure ratio are plotted versus downstream static pressure. At the beginning of decrease of the static pressure, the mass flow rate raises with high gradient. With further drop of backpressure the slope of the mass flow rate becomes less steep. Finally, in the range of 150 down to 125kPa, the rise of the flow rate is insignificant, reaching magnitude of 2.26kg/s. At the same time, pressure ratio drops with almost linear function, from 3.88:1 to 3.6:1. For the lowest, critical outlet static pressure of 125kPa, a supersonic flow occupies significant part of the blade channel. The outlet of the impeller is completely blocked by supersonic flow (Figure 15). Complete compressor choke map is presented in Figure 16. It reveals nonlinear relation between mass flow rate and pressure ratio, known from turbomachinery theory. The satisfying pressure ratio is achieved for mass flow not higher than 2.15kg/s. Above this value pressure ratio decreases drastically with important increment of deficiency.

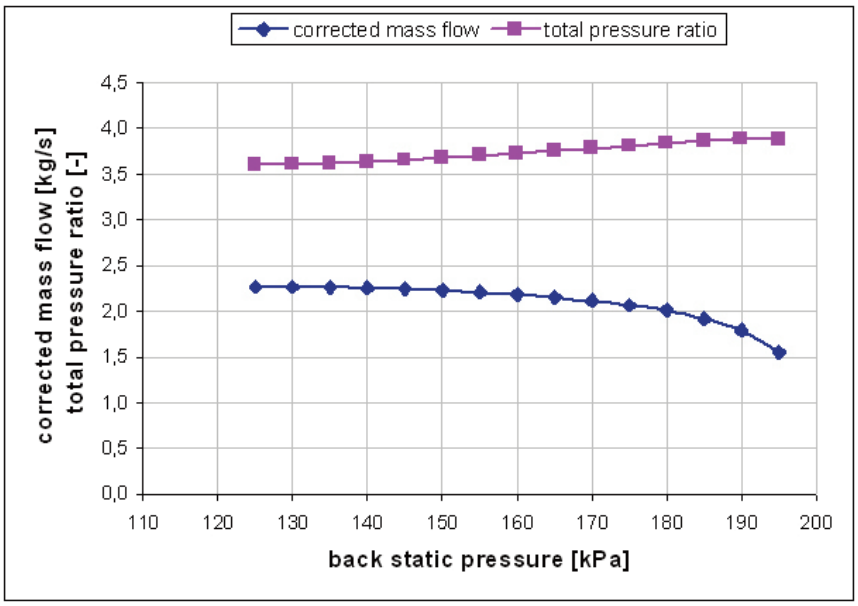

Figure 14. Mass flow and total pressure ratio as a function of backpressure

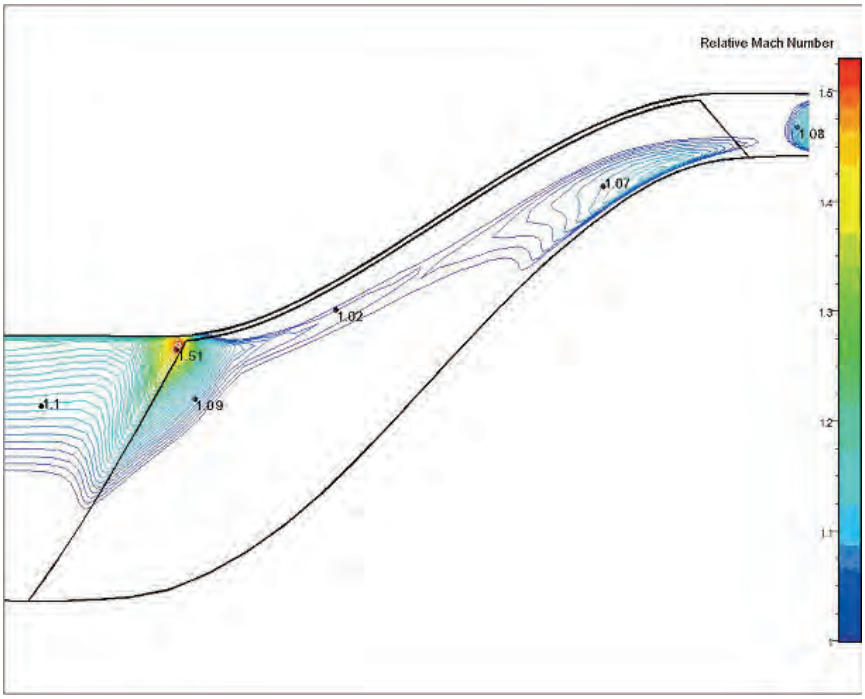

Figure 15. Critical conditions at the impeller outlet

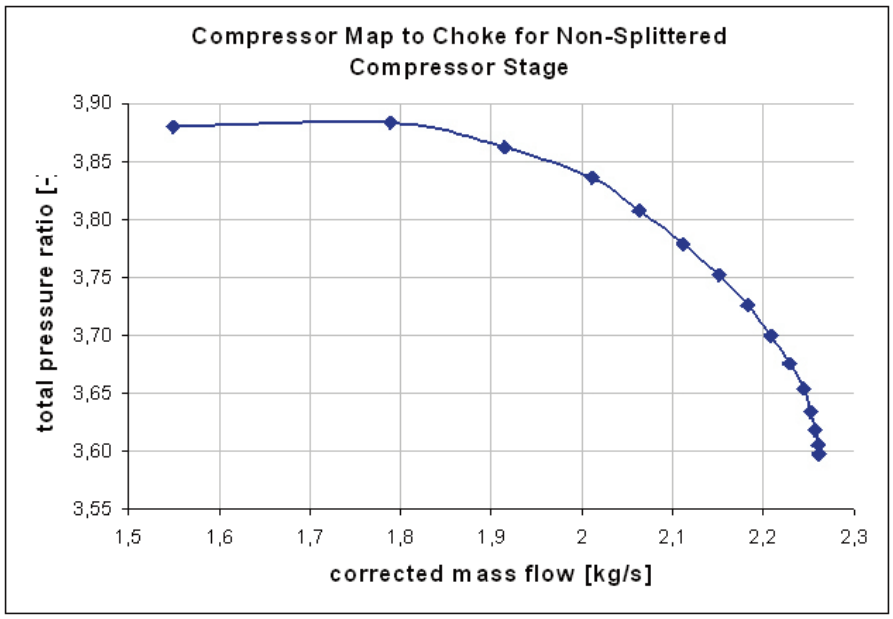

Figure 16. Compressor map to choke for the splittered compressor wheel

8. CONCLUSIONS

During this project several important compressor design issues were addressed. As a result of the initial modification of the centrifugal compressor, splitter blade has been removed. Numerical analysis proved better performance of the non-splittered version. Presence of splitter blade in the flow duct caused disturbed and swirled flow implying significant difference between divided flow passages. This effected lower pressure ratio and mass flow rate. The next improvement regarded to reduction of clearance on the blade tip. The relevant computations showed lower efficiency with increasing tip gap due to increased mixing losses and swirled flow within tip clearance. Linear relation between efficiency loss and tip clearance, obtained in numerical calculations, agreed with turbomachinery theory. The last stage of mixed-flow compressor CFD study provided choke flow predictions. By controlling outlet boundary conditions, a higher mass flow rate through the compressor was produced. As the effect of higher mass flow rate, the relative Mach number reached unity at the geometrical throat of the blade passage and choke flow occurred. Presented relations between mass flow rate and pressure ratio enabled to define upper limitations of stable operating range for the designed compressor.

List of Symbols

C	absolute velocity,
C_m	absolute meridional velocity,
C	absolute tangential velocity,
W	relative velocity,
W_m	relative meridional velocity,
W_θ	relative tangential velocity,
U	blade tip velocity,
h_0	stagnation enthalpy,
L	specific work,
T	static temperature,
T_0	stagnation temperature,
p	static pressure,
p_0	stagnation pressure,
γ	specific heat ratio,

M absolute Mach number,
η efficiency,
π pressure ratio,
τ temperature ratio,
N dimensionless speed,
Θ non-dimensional mass flow,
α absolute flow angle,
β relative flow angle,
β_b blade angle,
$\Delta\beta$ slip angle,
t_c tip clearance.

BIBLIOGRAPHY

[1] Cumpsty N.A., "Compressor Aerodynamics", Longman Scientific and Technical, 1989
[2] Japikse D. and Baines N.C., "Introduction to Turbomachinery", Concept ETI, Inc. and Oxford University Press, 1997
[3] Japikse D., "Centrifugal Compressor Design and Performance", Concept ETI, 1996
[4] Japikse D., "Decisive Factors in Advanced Centrifugal Compressor Design and Development", Concepts ETI, Inc. paper
[5] Krain H., "Flow in Centrifugal Compressors. Experimental Observation of the Flow in Impellers and Diffusers", Von Karman Institute for Fluid Dynamics. Lecture Series 1984-07, May 1984
[6] Fagana J.R. and Fleeter S., "Impeller Flow Filed Measurement and Analysis", The American Society of Mechanical Engineers paper 90-GT-146
[7] Krain H., Hoffmann B. and Pak H., „Aerodynamics of a Centrifugal Compressor Impeller with Transonic Inlet Conditions", the American Society of Mechanical Engineers paper 95-GT-79, 1995
[8] Witfield A. and Baines N.C., "Design of Radial Turbomachines", Longman Scientific and Technical, 1990

B. Bogucki

ANALIZA NUMERYCZNA PRZEPŁYWU W STOPNIU SPRĘŻARKI OSIOWO-PROMIENIOWEJ SAMOLOTU BEZZAŁOGOWEGO

Streszczenie

Sprężarki odśrodkowe, które straciły w ostatnich dekadach swoje zastosowanie w silnikach wojskowych samolotów załogowych, są często stosowane przy napędzie małych samolotów bezzałogowych. Ich relatywnie duży stopień sprężania z jednego stopnia przy jednocześnie małych wymiarach, umocniły ich pozycję w nowoczesnych konstrukcjach małych statków powietrznych. Przy dążeniu do poprawienia ich sprawności, konstruktorzy ciągle napotykają szereg niestacjonarnych i nieliniowych zjawisk, które wymagają ustawicznych badań.

Projekt prezentowany w tej pracy został przeprowadzony na uczelni Ecole Nationale Supérieure d'Ingénieurs of Constructions Aéronautiques (ENSICA) w Tuluzie, w ramach programy rozwoju silnika do samolotu bezzałogowego. Prace były współ prowadzone przez Wydział Mechaniki Płynów z tejże uczelni oraz przez firmę JPX z Francji. Celem pracy było przeprowadzenie analizy numerycznej rozwiązań konstrukcyjnych zaimplementowanych w sprężarce osiowo-promieniowej silnika T100 o ciągu 100kN.